REMOTE SENS. ENVIRON. 47:311–321 (1994)

Retrieval of Apparent Surface Reflectance from AVIRIS Data: A Comparison of Empirical Line, Radiative Transfer, and Spectral Mixture Methods

William H. Farrand, Robert B. Singer,† and Erzsébet Merényi†*

Three methods for converting Airborne Visible/Infrared Imaging Spectrometer (AVIRIS) radiance data to apparent surface reflectance were compared using data collected over the Lunar Crater Volcanic Field in Nevada and the Pavant Butte tuff cone in Utah. The methods examined were the empirical line method, radiative transfer modeling (using LOWTRAN 7), and spectral mixture analysis using reference endmembers. Of the three, the empirical line and spectral mixture methods both provided good results. The approach utilizing LOWTRAN 7 accentuates noise inherent in AVIRIS data and requires a very accurate estimate of atmospheric water.

INTRODUCTION

Airborne and spaceborne sensors operating in the visible to near infrared (0.4–2.4 μm) detect solar radiance reflected from the Earth's surface. This radiance is affected by its downward and upward passages through the atmosphere and by its interaction with the surface. Land scientists are primarily interested in the latter set of interactions because of the characteristic narrow band absorptions and continuum slopes and inflections in the reflectance spectra of rocks, soils, and vegetation.

Since the flight of the first Landsat, various methods have been developed to extract ground reflectance from sensor DN. It is advisable to think of the reflectance values retrieved from remotely sensed data as "apparent" reflectances since the physical state of the surface (i.e., solid or particulate) and its orientation will affect the absolute level of reflectance. Thus the low apparent reflectance of a given pixel could be due to a disadvantageous lighting geometry or to the surface materials within that area having a genuinely low reflectance. The problem of extracting apparent reflectance has become even more relevant with the development of imaging spectrometry (e.g., Vane and Goetz, 1988). Imaging spectrometers utilize tens or hundreds of narrow (typically 10 nm wide) contiguous channels. Such high spectral resolution makes possible the unambiguous identification of electronic and vibrational overtone mineral absorption features as well as chlorophyll and lignin–cellulose features in plant spectra.

The instrument considered in this report is the Airborne Visible/Infrared Imaging Spectrometer (AVIRIS). AVIRIS was conceived as a testbed for spaceborne imaging spectrometers such as the High Resolution Imaging Spectrometer (HIRIS) and was first flown in 1987. The 1987 flight season was devoted primarily to performance evaluation studies. Deficiencies in the instrument that were found in 1987 were corrected in 1988, paving the way for the first operational flight season in 1989.

The NASA-sponsored Geologic Remote Sensing Field Experiment (GRSFE) took place in the summer of 1989. GRSFE was conceived and operated as a planetary mission with the unique twist that the planet under investigation was the Earth. GRSFE provided an opportunity to match the output from several state-of-the-art remote sensing systems against ground and atmospheric values measured concurrently with the over flights. The

*Science Applications International Corporation, Falls Church, Virginia

†Planetary Image Research Laboratory, University of Arizona, Tucson

Address correspondence to William H. Farrand, Science Applications International Corp., 803 W. Broad St., Ste. 100, Falls Church, VA 22046.

Received 27 August 1992; revised 8 June 1993.

0034-4257/94/$7.00

655 Avenue of the Americas, New York, NY 10010

Table 1. AVIRIS Characteristics

	Overall Instrument		
IFOV	0.95 mrad		
GIFOV	20 m		
FOV	30°		
Swath	10.5 km		
	Individual Spectrometers		
Spectrometer	*Spectral Range (μm)*[a]	*Sampling Interval (μm)*	*SN*[a,b]
A	0.3969–0.7027	9.6–10.1	150:1
B	0.6747–1.283	8.8–9.2	140:1
C	1.244–1.867	9.7–10.0	70:1
D	1.830–2.454	9.9–11.5	30:1

[a] The wavelengths and bandpasses within each spectrometer were determined from a mailing that accompanied that data tapes holding the late 1989 AVIRIS data. After each recalibration of the instrument, these values change somewhat.

[b] Signal:noise values taken from Vane (1987). The quoted values are laboratory values. Actual values would vary within any given flight season and according to the ground albedo.

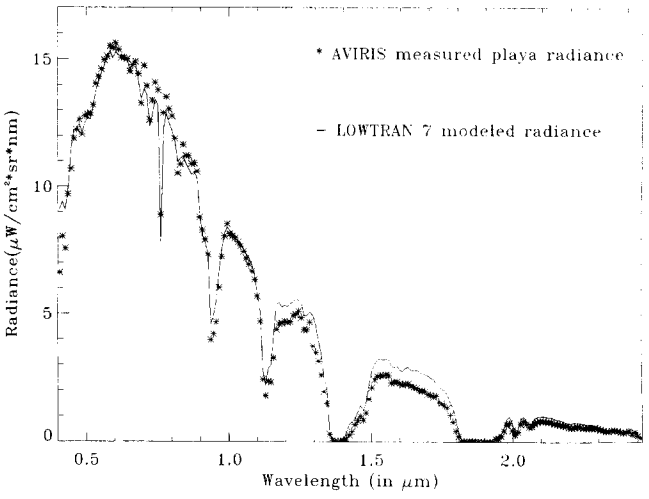

Figure 1. Radiance of Lunar Lake playa as measured by AVIRIS compared with the model radiance derived from LOWTRAN 7. The LOWTRAN 7 spectrum was initially of higher spectral resolution, but was convolved down to AVIRIS band widths.

concurrent collection of surface and airborne data provided the opportunity to validate the quantitative extraction of surface properties such as reflectance and emittance from the remotely sensed data.

In this study, results are presented for AVIRIS data collected over the primary GRSFE field area, the Lunar Crater Volcanic Field (LCVF) of northern Nye County, Nevada. AVIRIS data is also presented in this study for a scene of the Pavant Butte tuff cone in Millard County, Utah. Three methods of converting image DN to apparent ground reflectance were examined in this study. These were the empirical line method, radiative transfer modeling, and a spectral mixture analysis using library reference spectra.

THE AVIRIS INSTRUMENT

AVIRIS is flown on board the NASA ER-2 aircraft at an altitude of approximately 20 km. The instrument operates in the 0.4–2.45 μm region collecting 224 channels with a nominal spectral bandpass of 10 nm. After eliminating spectral overlap, there are 210 spectrally unique channels. These and other characteristics of AVIRIS are provided in Table 1.

AVIRIS data are available to investigators in a format with DN equal to radiance. Figure 1 shows the radiance spectrum for a 6 × 6 pixel area on the Lunar Lake playa. Also shown in Figure 1 is the LOWTRAN 7 modeled radiance (see below) of Lunar Lake,[1] convolved to AVIRIS bandpasses, for that particular AVIRIS scene. A full description of the radiometric calibration of AVIRIS is given by Green et al. (1991).

The AVIRIS data presented here for the LCVF were collected as part of the Geologic Remote Sensing Field Experiment on 29 September 1989 on GRSFE flight line 2, run 2 at approximately 11:44 PDT. The Pavant Butte data were collected on 27 September 1989 at 2:14 PDT as part of a Geosat Committee sponsored investigation of the nearby Drum Mountains.

METHODS

Assumptions Inherent in Conversions to Reflectance

All the methods examined below are limited by some common assumptions. These assumptions are made largely in order to simplify the theoretical and computational task of converting at-sensor radiance to apparent surface reflectance for each pixel in an AVIRIS image. The first of these assumptions is that of atmospheric uniformity. It has been demonstrated by Gao et al. (1991) that the amount of total column water vapor varies across an AVIRIS scene. However, for areas with subdued topography, the relative level of variability is low, on the order of 20% or less variation in precipitable water (Green, 1991; Gao et al., 1991); thus the assumption of atmospheric uniformity across an AVIRIS scene (12.8 km × 10.2 km) is often acceptable.

For scenes with substantial topographic relief, there are accompanying differences in atmospheric path length. These differences impact adversely on methods which

[1] The version of LOWTRAN 7 used had been modified to accept reflectance spectra instead of a flat surface albedo value. Thus the LOWTRAN 7 modeled radiance shown in Figure 1 was based on a simulation of solar radiation incident on the playa surface with a reflectance that was measured in the field with the PIDAS field spectrometer.

use the surface as a reference (e.g., the empirical line method and reference endmember modeling) if the reference areas in the image are at substantially different elevations than the areas of interest. This assumption is also a problem for the LOWTRAN 7 reflectance conversion unless LOWTRAN 7 is run with a different input atmospheric path length for each pixel, a computational intensive task. In the scenes examined below, topography is relatively subdued with differences in elevation of less than 0.5 km.

The primary disadvantage of not correcting for variations in atmospheric path length or nonuniformity within a scene is that the retrieved reflectances at and around water absorption features will be erroneous. This will be most notable at the 0.94 μm and 1.13 μm features and also at the wings of the more profound 1.4 μm and 1.9 μm features. For applications such as mineralogic or vegetative mapping, this will not be an impediment. For more sophisticated applications that seek to use hyperspectral data to determine leaf water content and/or surface moisture (e.g., Green et al., 1991; Gao et al., 1991), errors in the reflectance at these water features will be extremely detrimental. Such applications will of necessity have to utilize radiative transfer techniques that can determine column water abundance on a pixel-by-pixel basis. Naturally such methods require far greater blocks of computer time than the methods which assume a single set of correction factors for the entire scene.

Topography accounts for a third assumption—that pixels are viewed from similar perspectives. As was alluded to earlier, a level surface's photometric properties can dictate that it will have a different apparent reflectance than a sloped surface of equivalent materials.

Empirical Line Method

The empirical line method for the recovery of surface reflectance has been described in numerous places (e.g., Conel and Alley, 1985; Roberts et al., 1986; Conel et al., 1987). The empirical line method is based on the following simplified equation:

$$\mathrm{DN}_b = \rho(\lambda)A_b + B_b, \qquad (1)$$

where DN_b equals the digital number for a given pixel in band b, $\rho(\lambda)$ equals the reflectance of the surface materials within the GIFOV of that pixel at the wavelength λ of band b, A_b equals the multiplicative term which affects the DN (transmittance and instrumental factors), and B_b equals the additive term (primarily atmospheric path radiance and instrumental offset, i.e., dark current). The empirical line method is used to solve for the gain values A_b and offset values B_b in Eq. (1). The method relies on the characterization of the surface reflectance within two or more areas of varying albedos that are compositionally as homogeneous as can be found.[2] This method is frequently applied with just one light and one dark target; then, for any band, a plot such as Figure 2 can be made wherein the image DN of one or more pixels covering the light and dark targets is plotted against the measured surface reflectance of those targets. The slope of the resulting line is the gain for that band and the y-intercept is the offset. Better statistics can be obtained by using more surface calibration targets. Four targets were used for the LCVF AVIRIS data. Gain and offset spectra were determined using a least squares fitting technique. The Pavant Butte data were corrected using just two calibration targets.

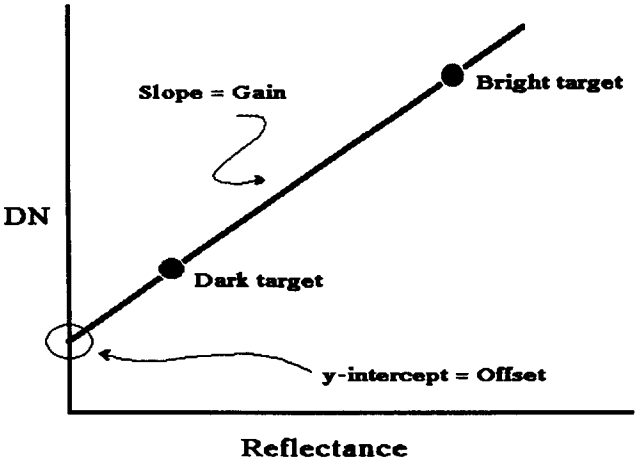

Figure 2. Gain and offset derived from a single channel via the empirical line method.

The values for ground reflectance of the calibration targets can be determined either with field spectrometers or by measuring the reflectance of representative samples in the laboratory. Coincident with the ER-2 overflights of the LCVF on 29 September 1989 measurements of the reflectance of the Lunar Lake playa were made with the Portable Instant Display and Analysis Spectrometer (PIDAS) (Goetz, 1987). Eighty measurements of the playa surface were made with a reference measurement of a Spectralon™ standard made after every four surface measurements for a total of 100 spectra. Measurements of basalt flows near Lunar Lake had been made on 17 July 1989 by a Single beam visible InfraRed Intelligent Spectrometer (SIRIS).

Laboratory measurements were made on samples of oxidized basaltic cinders and hydrovolcanic basaltic tuff from the Easy Chair Crater tuff and cinder cone. The reflectance of these samples were measured over a spectral range of 0.3–2.7 μm at the RELAB facility

[2] The more homogeneous the target, the easier it is to characterize the surface reflectance within the territory covered by several pixels using a field spectrometer.

at Brown University (Mustard and Pieters, 1989). The RELAB spectrometer measures bidirectional reflectance at user-defined phase angles with reference to a pressed halon standard. The cinder and tuff samples were measured at a phase angle of 42°, equivalent to the solar zenith angle extant at the time of the AVIRIS data collection.

Measurements of ground reflectance in the Pavant Butte area were made with PIDAS on 26 September 1989 approximately 1 hour before the AVIRIS overpass. The bright target was a small hard pan playa north of Pavant Butte. The dark target was a dark cinder strewn field south of Pavant Butte. Samples of the playa and dark cinders from the Pavant Butte area were also measured at RELAB, with the spectra again being acquired under a viewing geometry similar to that of the AVIRIS flight (phase angle = 48°). Thus an empirical line calibration was done for the Pavant Butte scene with both PIDAS and RELAB reflectance data.

Of the sample spectra acquired at RELAB, natural (i.e., weathered) surfaces were measured for the cinder samples collected at Easy Chair Crater and near Pavant Butte. The tuff and playa samples that were measured were powdered samples with grain sizes of 500 μm or less. It should be noted that measuring the tuff and playa materials as powders in the laboratory is not too dissimilar from viewing them in their natural occurrence as aggregated powders.

Radiative Transfer Modeling

The multiplicative and additive effects of atmospheric attenuation and scattering as well as the initial shape of the solar spectrum can be determined using a model of radiative transfer. LOWTRAN 7 (Kneizys et al., 1989) has been used by other authors (e.g., Carrere and Chadwick, 1990; Green, 1991) to calibrate AVIRIS data to reflectance. The method followed by Green (1991) is based on the following equation:

$$\rho_{\text{AVIRIS}}(\lambda) = \frac{L_{\text{AVIRIS}}(\lambda) - L_{\text{path}}(\lambda)}{L_{\text{Lambertian}}(\lambda)}, \quad (2)$$

where $L_{\text{AVIRIS}}(\lambda)$ is the radiance measured by AVIRIS, $L_{\text{path}}(\lambda)$ is the path radiance as calculated by LOWTRAN 7 for a 0% albedo surface, $L_{\text{Lambertian}}(\lambda)$ is the radiance reflected from a 100% albedo Lambertian surface as calculated by LOWTRAN 7, and $\rho_{\text{AVIRIS}}(\lambda)$ is the derived reflectance.

As inputs to the LOWTRAN 7 code, one can account for the illumination geometry of the scene (by specifying latitude, longitude, Julian date, and time of day). In order to account for atmospheric effects, one of several standard atmospheric profiles can be used (e.g., midlatitude summer) and site elevations other than sea level can also be taken into account. The version of LOWTRAN 7 used is a version modified at the NASA Jet Propulsion Laboratory to accept scaling factors for atmospheric H_2O, CO_2, O_2, O_3, CH_4, and SO_2. For the given gas species, the specified scaling factor will reduce or enlarge the proportion of that species in each level of the specified model atmosphere. For example, a scaling factor of 0.5 for H_2O will halve the H_2O abundance in each atmospheric layer considered in the radiative transfer model. As part of the 29 September GRSFE efforts, two radiosondes were launched, and measurements were taken during the time of the over flights with a 10-channel sunphotometer and two two-channel ratioing spectral hygrometers (Bruegge et al., 1990). No atmospheric information was obtained in conjunction with the 26 September Pavant Butte overflight.

In order to run LOWTRAN 7 for the conditions extant at the time of the GRSFE AVIRIS data collection, the location of the LCVF, its elevation, and the time of data acquisition were all entered into the program. Optical depth was obtained from the sunphotometer measurements [following the method of Bruegge (1985)] and this was used to obtain a value of 31.3 km for visibility that was entered into the program. The best results were obtained using temperature, pressure, and atmospheric gas profiles (with the exception of water vapor) from the midlatitude summer standard atmospheric profile. The program was run at a spectral resolution of 20 cm^{-1}, which, at short wavelengths, is greater than that of AVIRIS. Results presented in the figures are convolved to AVIRIS bandpasses.

Several approaches to estimating atmospheric water were examined. The idea of using the radiosonde data to generate a model atmosphere was considered and rejected on the basis of the questionable reliability of relative humidity measurements provided by such instruments (Bruegge et al., 1990). Spectral hygrometer measurements provided a total column water abundance value of 0.9 cm over Lunar Lake. Initial runs of LOWTRAN 7 with this value provided apparent reflectance spectra with positive 0.94 μm and 1.13 μm water features, thereby indicating that a lower water value was in order. Consequently, total column water abundance was calculated from the AVIRIS data itself as a percentage of that in the midlatitude summer model using the CIBR method (Carrere et al., 1990).

The CIBR method makes use of the continuum interpolated band ratio (CIBR) across the 0.94 μm or 1.13 μm feature in the radiometrically calibrated AVIRIS data. CIBR is defined as

$$\text{CIBR} = L_{\text{band center}} / (C_1 L_1 + C_2 L_2), \quad (3)$$

where $L_{\text{band center}}$ is the radiance at the center of the water absorption band, L_1 is the radiance at the short wavelength shoulder of the water absorption band, and L_2 is the radiance at the long wavelength shoulder. C_1 and C_2 are constants related to AVIRIS bandwidth. For the 0.94 μm feature where bandwidth is equal across

the absorption band, C_1 and C_2 are both 0.5. For the 1.13 μm feature, C_1 is 0.52 and C_2 is 0.48 (Carrere et al., 1990). In the CIBR method, LOWTRAN is run for several values of atmospheric water given the viewing geometry and altitude of a given AVIRIS scene. A growth curve of the form

$$\text{CIBR} = \exp(-\alpha w^{\beta}) \tag{4}$$

results, where w is the amount of water and α and β are constants specific to the growth curve determined by the CIBR method.

CIBR is essentially the inverse of band depth (BD), which as defined by Clark and Roush (1984), is

$$\text{BD} = 1.0 - \text{BC} / C_{\text{BC}} \tag{5}$$

where BC is the reflectance or radiance value at band center and C_{BC} equals the continuum value over band center. In this study, CIBR of the 0.94 μm water feature was determined over runs of LOWTRAN from 5% to 120% of the column water in the midlatitude summer model. A plot of 0.94 μm CIBR vs. % water is shown in Figure 3. Using the curve in Figure 3, the column water abundance over a given area in the AVIRIS scene could be determined by relating the 0.94 μm CIBR for that area to percent water. The CIBR method produced an estimate of approximately 74% of the midlatitude summer model column water abundance (approximately 0.59 pr cm) over the Lunar Lake playa. This calculation was also done with band depth values for the 0.94 μm water band retrieved using the SPECPR program (Clark et al., 1990). As expected, this approach also produced an estimate of 0.59 pr cm over Lunar Lake.

It is assumed that surface reflectance varies linearly with wavelength across the spectral region encompassing the 0.94 μm and 1.13 μm water bands. Over Lunar Lake this is a valid assumption; however, the cinders composing Easy Chair Crater are coated with ferric oxides. The continuum depression caused by the Fe^{3+} band near 0.9 μm is likely to skew the predicted column water abundance by using the 0.94 μm band alone. Thus over Easy Chair Crater, % water was calculated as the average predicted by the 0.94 μm and 1.13 μm curves of growth.

For the Easy Chair Crater site, the LOWTRAN 7 correction technique was run with the same input parameters except for a surface elevation of 2.0 km rather than the 1.75 km elevation of Lunar Lake, which means a different input water scaling factor (again determined from the CIBR method).

Figure 3. Plot of 0.94 μm CIBR vs. the percent of water vapor contained in the midlatitude summer LOWTRAN 7 model. A CIBR of 0.41 observed in AVIRIS data over Lunar Lake indicates 74% of the water contained in the midlatitude summer model.

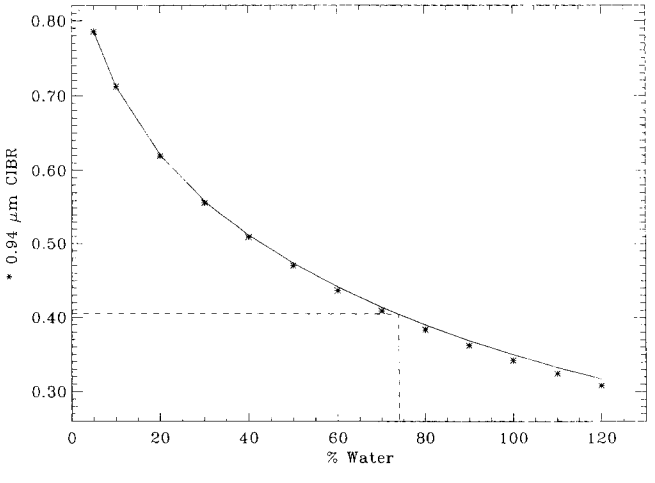

Spectral Mixture Modeling

There are two varieties of spectral mixtures: *macroscopic* and *intimate*. Macroscopic mixtures result when there is only a single set of interactions between surface materials and photons. That is, a given photon will be reflected (or absorbed) by only one type of material. Singer and McCord (1979) described this as a "checkerboard" mixture since the fractions of endmember materials could equate to proportionate areal exposures of those endmembers. *Intimate* mixtures occur when individual photons interact with more than one type of material. The reflected radiance of "checkerboard" exposures of materials (i.e., macroscopic mixtures) combine in an additive fashion producing a linear set of equations. Intimate mixtures are nonlinear.

The spectral mixture modeling method used in this study is a linear model that has been developed by Smith et al. (1987; 1990). A more complete description of spectral mixture analysis can be found in Gillespie et al. (1990). The method is based on the assumption that virtually all of the spectral variation in a multi- or hyperspectral data set can be accounted for by a relatively small number of endmember spectra. In this context, an "endmember" is taken to be a spectrum that defines an end or corner of a mixing line or space. Pixels that contain a substantial fraction of materials whose reflectance causes the pixel's reflectance signature to deviate from the model contribute to the residuals generated by the method.

Spectral mixture analysis can be used as a tool both for scene classification as well as for relating image DN or radiance to surface reflectance. In the first stage of spectral mixture analysis, the spectral variability of the image is modeled by several *image endmembers*. An image endmember or *iem* is the encoded radiance spectrum of one or more pixels which cover an area, or areas, in the image data that is representative of a unique type of surface material. Generally, several materials contribute to the radiance spectrum of any one *iem*.

Image endmembers are determined in an iterative

procedure. An initial set of *iem* candidates are used to compute, over all bands, the fractional contributions of these endmembers within each pixel. This is done by solving the following equation system for each pixel independently:

$$L_b = \sum_{i=1}^{N} F_i L_{i,b} + E_b \text{ for } b = 1, \ldots, M \text{ and } \sum_{i=1}^{N} F_i = 1 \quad (6)$$

such that the sum of the squared error terms E_b is minimized. F_i is the fraction of endmember i; L_b is the observed radiance in band b. $L_{i,b}$ is the radiance that endmember i is contributing in band b; E_b is the residual for band b; M is the number of bands; and both summations are carried from $i = 1$ to N, where N is the number of endmembers. If the error is uniformly low over the modeled scene and the fraction values are reasonable (clustering between 0 and 1), then the choice of the *iems* is satisfactory; otherwise the *iems* need to be modified by adding more and / or selecting different ones.

With M bands, the number of endmembers is constrained to be no greater than $M + 1$. Even for multispectral systems such as the Landsat TM, this limit is seldom reached. For a system such as AVIRIS there is actually a surfeit of channels. Since this is the case, it is advisable to delete the channels with the lowest signal / noise. These bands tend to be the shortest and longest wavelength channels and those channels in the middle of atmospheric water absorption bands. Even though signal / noise is poor in the long wavelength channels (i.e., the 2.2–2.3 μm region), many of these channels are included since key mineralogic absorptions occur in this spectral region.

Once all the image endmembers have been determined, a library of laboratory and / or field spectra can be used to determine the composition of the *iems* in terms of known reference spectra. The reference endmember, or *rem*, is ideally the major component of the corresponding *iem*, but conceivably a material with a similar reflectance spectrum could be used as a proxy. In the process of relating *iems* to *rems*, a set of gains and offsets are calculated which can be used to transform image DN to reflectance. This procedure of *reference endmember modeling* was followed in order to obtain ground reflectance.

Note that this procedure allows for heterogeneous surface areas to be used as calibration targets. Even a heterogeneous area can be used as an *iem*. This area can then be described in terms of component *rems*, thereby relating the heterogeneous surface area seen in the image to homogenous, well-characterized reference materials.

The equation system that describes this modeling process is as follows, for each band b separately:

$$G_b L_{i,b} + O_b = \sum_{j=1}^{N} F_{j,i} \rho_{j,b} + E_b, \quad i = 1, \ldots, N$$

$$\text{with the constraint that } \sum_{j=1}^{N} F_{j,i} = 1, \quad (7)$$

where $L_{i,b}$ is the radiance in band b for image endmember i, G_b and O_b are respectively the gain and offset in band b, $\rho_{j,b}$ is the laboratory or field reflectance of reference endmember j in band b, $F_{j,i}$ is the fraction of reference endmember j in image endmember i, E_b is the residual in band b, and N is the number of endmembers. Since in (7) G_b, O_b, and $F_{j,i}$ are all unknown at the beginning, a sequence of calculations is begun in which it is initially assumed that each *iem* is composed entirely of the corresponding *rem*. A preliminary set of G_b and O_b values are generated which can be used to determine the fractional contributions of the *rems* to each *iem*. Model *rems* constructed according to the calculated fractions can be used in place of the actual reference spectra in a repeat of the first step in order to produce a more accurate set of gains and offsets. This procedure can then be repeated, alternating between the left hand and right hand side until the errors are minimized.

As was the case with the gains generated by the empirical line method, the values G_b account for multiplicative effects such as instrumental gain and atmospheric transmissivity. Likewise, the values O_b account for additive effects such as instrumental offsets and atmospheric path radiance.

The implementation of Eq. (7) which was used in this study was based on programs originally written at the University of Washington (M. Smith, personal communication) and modified at the University of Arizona. These programs have the capability to search through a spectral library of potential reference spectra and select those spectra which most closely resemble the image endmembers. For the LCVF scene, four endmembers were used: shade,[3] playa, cinder, and rhyolite. The playa and cinder reference spectra were those used in the empirical line calibration described above. While the "rhyolite" (the geologic unit from which this *iem* was selected is actually a poorly- to moderately well-welded rhyolitic tuff) was compared with several rhyolitic tuff reflectance spectra, the closest spectral analog in the available spectral library was an Easy Chair Crater basaltic tuff reflectance spectrum. For the Pavant Butte scene, five endmembers were used: shade, playa, palagonite tuff, vegetation, and red soil. Shade was modeled initially by a constant reflectance of 0.01. In the second iteration of Eq. (7), the "shade" *rem* included fractional contributions of the other *rems* and thus the shade "reflectance" varied with wavelength in a fashion more consistent with the observed *iem*. The playa spectra used in both cases were measured by PIDAS in the field, and three of the four other reference spectra were RELAB sample spectra measured as powdered samples (again for playa, tuff and soil samples, this is not unlike their natural state). The fourth *rem*

[3] The concept of a "shade" endmember is discussed by Adams et al. (1986) and Gillespie et al. (1990).

was a black brush (*Coleogyne ramosissima*) leaf spectrum measured in hemispherical reflectance on the University of Washington Beckman DK-2A spectrophotometer. This final endmember was selected by the software from several leaf reflectance spectra as the type of vegetation most resembling the Pavant Butte vegetation image endmember.

RESULTS

Before delving into the relative merits of the various calibration techniques, a brief discussion of the criteria of a good reflectance calibration is in order. For geologic remote sensing, the most important aspects are often the overall shape of the spectrum and the position and shape of specific mineralogic absorption features. Similarly, it has been shown that vegetation can be mapped on the basis of the location and shape of the 0.55 μm "green peak" (Clark et al., 1992). For other purposes, obtaining a quantitative estimate of the level of reflectance is also important.

Figure 4a shows a comparison of retrieved reflectances of the Lunar Lake playa as calculated by the three methods described above; Figure 4b compares reflectances of oxidized basaltic cinders at Easy Chair Crater. Figure 5 shows a comparison of reflectance spectra of palagonite tuffs retrieved from the AVIRIS data by the empirical line and spectral mixture methods for Pavant Butte. In each figure, a representative field or laboratory spectrum is included for purposes of comparison.

The spectra with the greatest scatter in Figure 4 are the spectra calibrated to reflectance by LOWTRAN 7. This calibration technique tends to accentuate the noise inherent in AVIRIS data. The gain spectra calculated by the other two methods are derived in part from the AVIRIS data itself. Thus for a given band, both pixel DN_b and the corresponding gain factor A_b [from Eq. (1)] share a common noise component which is removed from the ultimate reflectance value by dividing DN_b by A_b. With LOWTRAN 7 the original noisy data is divided through by a noise-free model spectrum with the result that noise inherent in the data becomes more apparent. It should be noted that the performance of AVIRIS has been substantially improved in recent flight seasons (Green et al., 1992). Thus, the noise component revealed

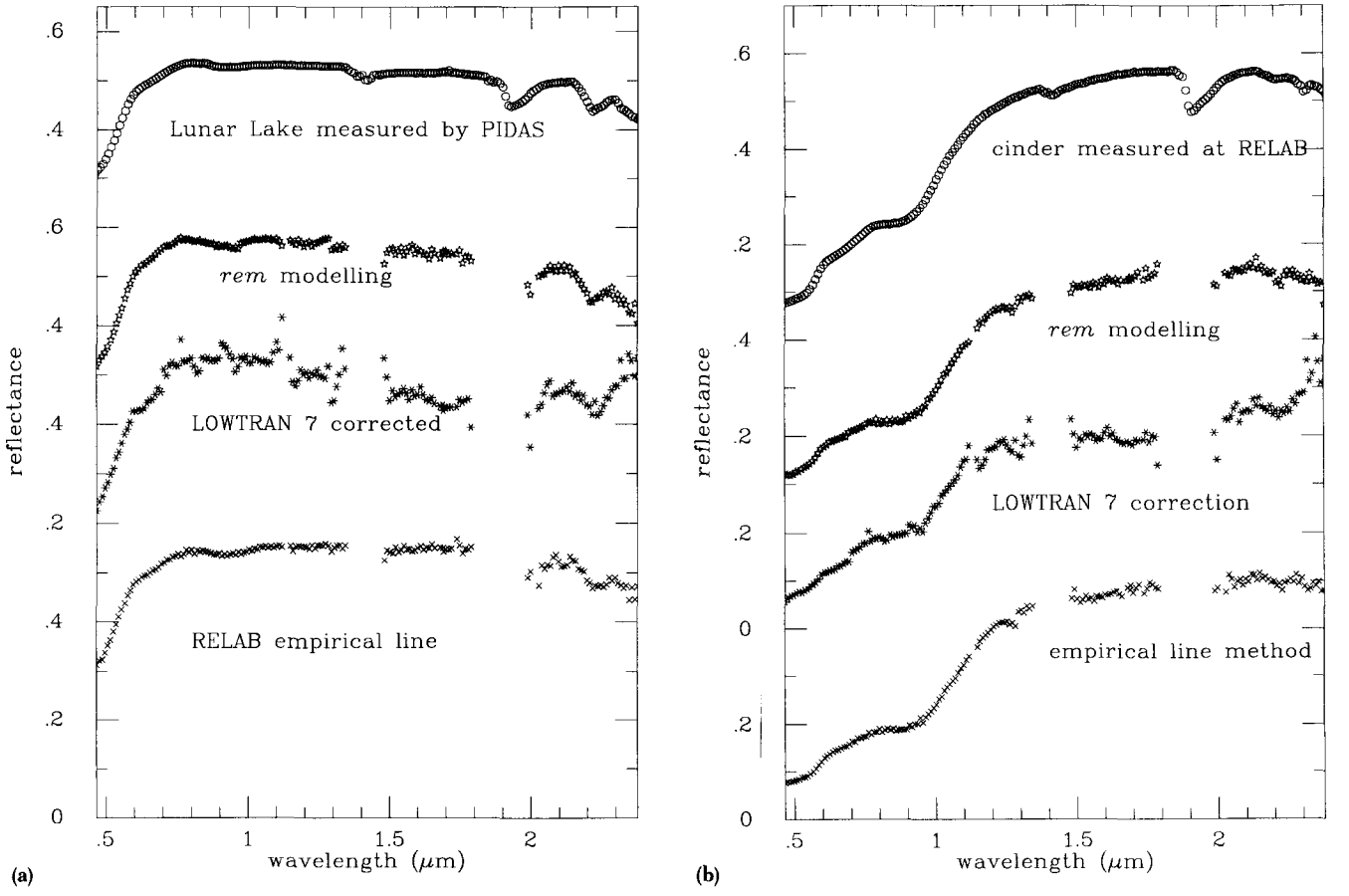

Figure 4. a) Comparison of Lunar Lake playa reflectance spectra. For the spectra derived from AVIRIS data, 158 channels are shown. The shortest and longest wavelength channels as well as those channels in the middle of atmospheric water absorptions have been deleted due to their poor signal / noise performance. The playa spectrum measured by PIDAS is presented at AVIRIS bandwidths. b) Comparison of Easy Chair Crater oxidized cinder reflectance spectra.

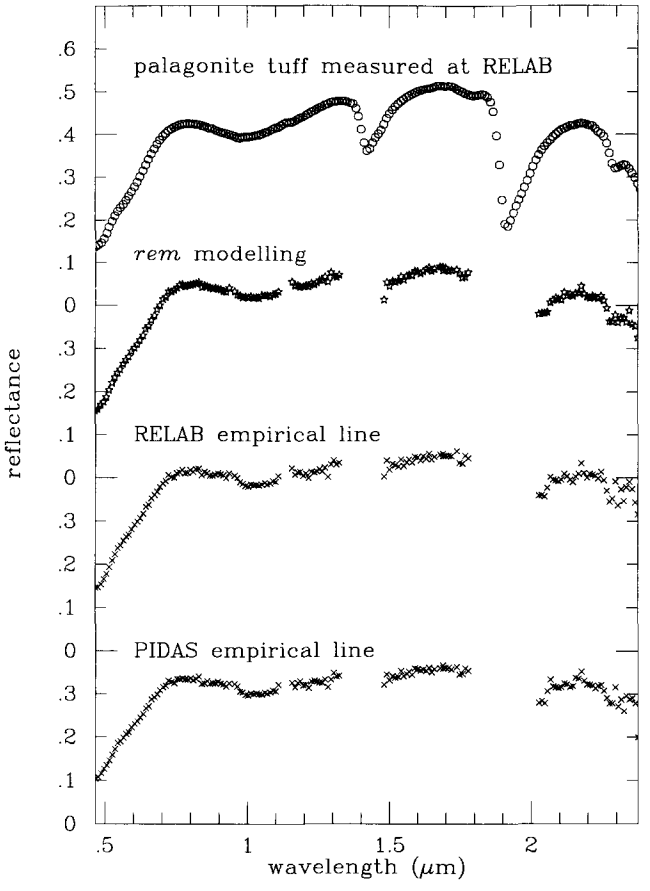

Figure 5. Comparison of Pavant Butte palagonite tuff reflectance spectra. For this AVIRIS scene, 150 channels were utilized. A calibration to reflectance utilizing LOWTRAN 7 was not attempted for this scene due to the lack of measured atmospheric properties from the day of the data collection.

by a LOWTRAN 7 or MODTRAN (Berk et al., 1989) correction should not be as significant in 1992 AVIRIS data as that observed in the 1989 data.

As has been mentioned by Green (1990) and Carrere and Chadwick (1990), reflectance calibrations done with LOWTRAN 7 are also very sensitive to atmospheric water content. If the model atmosphere has more water than the atmosphere which the sensor was actually looking through, water absorptions will appear as positive features on the derived reflectance spectrum. If the reverse situation were true, water absorptions could appear where the actual material did not have them. Over- or undercompensation of water features can also occur for scenes calibrated by the empirical line or the *rem* modeling method when a given area in the image is at a substantially different elevation than the reference surfaces.

While the LOWTRAN 7 corrected spectrum accounted for the 0.94 μm feature, it overcompensated for the 1.13 μm water absorption in both the Lunar Lake and Easy Chair Crater spectra. The overcompensation of the 1.13 μm water band is indicative of a persistent problem with column water abundance retrieval using AVIRIS data. In the 1989 LCVF data, there is a 24% difference between the column water abundance retrieved using the CIBR method from the 0.94 μm water band and from the 1.13 μm feature. While the performance of AVIRIS has been substantially improved in recent years, this mismatch between the water abundances persists. An examination of a 1992 AVIRIS data set collected over Mono Lake, California in September 1992 shows a mismatch of 16% in water abundances retrieved from the 0.94 μm and 1.13 μm water bands using the CIBR technique (Farrand, 1992, unpublished data). Figure 1 of Green et al. (1992) shows an offset of approximately 9% between AVIRIS measured and MODTRAN modeled radiance over the Ivanpah Playa in California on the long wavelength shoulder of the 1.13 μm water band.[4] This offset can account for some of the observed disparity since the CIBR technique relies critically on radiance values derived from the shoulders of the water absorption bands. Differences in column water abundance retrieved from the 0.94 μm and 1.13 μm water bands may be lessened by use of a curve fitting technique for the retrieval of atmospheric column water abundance (Green et al., 1993).

The reflectance spectra of the Lunar Lake playa derived from the empirical line method and *rem* modeling more closely resemble the PIDAS measured spectrum. The reflectance values derived from both the empirical line and the *rem* modeling methods are marginally higher than those measured by PIDAS. At longer wavelengths, the *rem* modeling spectrum has less scatter than either of the other two derived reflectance spectra. Note its excellent retrieval of the 2.2 μm Al–OH vibrational absorption.

For the Easy Chair Crater cinder spectra in Figure 4b, the *rem* modeling and the empirical line method results are comparable. The RELAB sample spectrum of oxidized cinder from Easy Chair Crater shows a rise in reflectance between the absorption edge at 0.55 μm and the 0.87 μm Fe^{3+} crystal-field absorption. This plateau is clearly evident in the reflectance spectrum derived by *rem* modeling and by the empirical line method but is less apparent in the LOWTRAN 7 corrected spectrum.

In Figure 5 the results from the empirical line calibration (done from RELAB spectra) very closely resemble the *rem* modeling results and the laboratory

[4] It is not clear whether the difference between the AVIRIS-measured and LOWTRAN-modeled radiance is due to a flaw in the radiometric calibration of AVIRIS or in the LOWTRAN database. We suspect the latter. Even line-by-line codes have been shown to produce line-to-line variations in retrieved water column abundance (Bruegge et al., 1990).

spectrum. However, the two empirical line calibration attempts in Figure 5 demonstrate how much that method is influenced by the type of bright and dark target spectra that are input. The calibration done with PIDAS data at Pavant Butte resulted in a lower overall reflectance than the empirical line calibration done from RELAB spectra or the *rem* modeling. While the latter two derived reflectance spectra appear similar, the scatter in the data points of the empirical line method calibration is greater than that which resulted from the *rem* modeling (this difference is most noticeable at longer wavelengths). To compare the two calibration methods over a larger portion of the image, part of the Pavant Butte AVIRIS image was converted to reflectance via the gains and offsets calculated from the empirical line (RELAB) and the *rem* modeling calibrations. A uniform 9×9 pixel region on a playa north of Pavant Butte had a higher standard deviation (over all 150 channels used in the analysis) for the empirical line calibration than for the *rem* modeling method.

CONCLUSIONS

Of the three methods considered here, reference endmember modeling yielded the best overall results. The least satisfactory method was radiative transfer modeling with LOWTRAN 7. Problems inherent in the LOWTRAN 7 reflectance retrieval method employed here include its sensitivity to atmospheric water content and the fact that it accentuates the noise within AVIRIS imagery. The problems encountered with the LOWTRAN 7 based method may be indicative of an inherent limitation in band model radiative transfer codes. More sophisticated band models such as MODTRAN (Berk et al., 1989) may obviate the problems encountered with LOWTRAN 7, but the ultimate solution may necessitate going to computationally intensive line-by-line codes [e.g., FASCODE and ATMOS (Brown et al., 1987)].

The empirical line and *rem* modeling reflectance retrieval methods yielded generally comparable results. The better results obtained at the LCVF by the four-point empirical line method as opposed to the two-point Pavant Butte calibration highlights the improvement that using more ground calibration targets can provide.

It must be mentioned that these surface based methods rely on a single set of gain and offset spectra and thus are especially susceptible to atmospheric variability within a scene due either to topographically induced differences in atmospheric path length or inhomogeneities in water vapor abundance. Only a radiative transfer technique could be used on a pixel-by-pixel basis to solve for such effects. However, the great majority of applications do not require such a computationally intensive recourse.

There are several other reported methods for calibrating imaging spectrometer data to apparent surface reflectance which were not considered in this study. These other methods include flat fielding, a distributed flat field method (Crowley, 1990), and a residual or scene-averaged method (Conel et al., 1987).

An important aspect of the relative merits of reflectance calibrations is how much ground truth data is needed to perform the calibration. Ideally, reflectance retrieval could be performed without having to travel out into the field in order to make ground truth measurements. The methods mentioned in the preceding paragraph can be used in this manner, although the authors cited (Crowley, 1990; Conel et al., 1987) who evaluated those methods found severe shortcomings. Making atmospheric measurements near the time of data collection appears crucial for the success of the LOWTRAN 7 based calibration. While the use of the CIBR method of (Carrere et al., 1990) appears to obviate the necessity of making radiosonde or spectral hygrometer measurements, the need to accurately estimate optical depth (most effectively done by sunphotometer measurements on the day of data collection) remains. It was shown that laboratory spectra can be used for the *rem* modeling method. In fact, given a comprehensive spectral library the need for collecting new ground measurements for each scene can be reduced by *rem* modeling since the *rems* chosen need only be analogous to the spectra of the *iems* they represent. That is, an *iem* could be modeled by the spectrum of a different material provided that material's reflectance matched the reflectance of the *iem*. This flexibility obviates the necessity of making extensive measurements of a calibration target since even a heterogeneous target can be represented by a mixture of reference spectra. Thus of the methods considered here, *rem* modeling offers the most promise for efficient reflectance retrieval with a minimum of ground truth field work.

The authors would like to thank the organizers of GRSFE, principally R. E. Arvidson and D. L. Evans of JPL, for making much of this work possible. The SIRIS data used was obtained from the GRSFE CD-ROM set released by the National Space Science Data Center. The spectral mixture modeling approach discussed here was developed at the University of Washington by J. B. Adams, M. O. Smith, and others. We thank them for their invaluable help. The Pavant Butte AVIRIS and PIDAS data were made available by G. B. Bailey of the USGS at Sioux Falls. Thanks to Ron Alley of JPL for providing their modified version of LOWTRAN 7. Thanks also to Steve Pratt at Brown University's RELAB for measuring the laboratory spectra used in this work. Data processing and analysis were performed at the University of Arizona's Planetary Image Research Laboratory. This work was funded in part by NASA Grant NAGW-1059.

REFERENCES

Adams, J. B., Smith, M. O., and Johnson, P. (1986), Spectral mixture modeling, a new analysis of rock and soil types at

the Viking Lander 1 site, *J. Geophys. Res.* 91(B8):B8098–B8112.

Berk, A., Bernstein, L. S., and Roberson, D. C. (1989), *MODTRAN: A Moderate Resolution Model for LOWTRAN 7*, U.S. Air Force Geophysical Laboratory, Hanscom Air Force Base, MA.

Blount, G., Smith, M. O., Adams, J. B., Greeley, R., and Christensen, P. R. (1990), Regional aeolian dynamics and sand mixing in the Gran Desierto: Evidence from Landsat Thematic Mapper images, *J. Geophys. Res.* 95:15,463–15,482.

Brown, L. R., Farmer, C. B., Rinola, C. P., and Toth, R. A. (1987), Molecular line parameters for the Atmospheric Trace Molecular Spectroscopy experiment, *Appl. Opt.* 26: 515.

Bruegge, C. J. (1985), In-flight absolute radiometric calibration of the Landsat Thematic Mapper, Ph.D. dissertation, University of Arizona (published under Kastner).

Bruegge, C. J., Conel, J. E., Margolis, J. S., Green, R. O., Toon, G., Carrere, V., Holm, R. G., and Hoover, G. (1990), In-situ atmospheric water-vapor retrieval in support of AVIRIS validation, in *Imaging Spectroscopy of the Terrestrial Environment*, SPIE 1298, SPIE, Bellingham, WA, pp. 150–163.

Carrere, V., Conel, J. E., Green, R. O., Bruegge, J. C., Margolis, J. S., and Alley, R. E. (1990), Analysis of atmospheric water vapor maps from AVIRIS at Salton Sea, California: Part I, experiments, methods results and error budgets, in *Proc. 2nd Airborne Visible / Infrared Imaging Spectrometer (AVIRIS) Workshop* (R. O. Green, Ed.), JPL Publication 90-54, Jet Propulsion Laboratory, Pasadena, CA, pp. 107–128.

Carrere, V., and Chadwick, O. (1990), An AVIRIS survey of Quaternary surfaces formed on carbonate provenance alluvium, Mojave Desert, southern Nevada, in *Proc. 2nd Airborne Visible / Infrared Imaging Spectrometer (AVIRIS) Workshop* (R. O. Green, Ed.), JPL Publication 90-54, Jet Propulsion Laboratory, Pasadena, CA, pp. 82–93.

Chrien, T. G., Green, R. O., and Eastwood, M. I. (1990), Accuracy of the spectral and radiometric laboratory calibration of the Airborne Visible / Infrared Imaging Spectrometer, in *Imaging Spectroscopy of the Terrestrial Environment*, SPIE 1298, SPIE, Bellingham, WA, pp. 37–49.

Clark, R. N., and Roush, T. L. (1984), Reflectance spectroscopy: quantitative analysis techniques for remote sensing applications, *J. Geophys. Res.* 89:6329–6340.

Clark, R. N., Swayze, G. A., King, T. V. V., Middlebrook, B., Calvin, W. M., and Gorelick, N. (1990), The U.S. Geological Survey, digital spectral library and analysis software, in *Proc. 2nd Airborne Visible / Infrared Imaging Spectrometer (AVIRIS) Workshop* (R. O. Green, Ed.), JPL Publication 90-54, Jet Propulsion Laboratory, Pasadena, CA, pp. 208–215.

Clark, R. N., Swayze, G. A., Koch, C., and Ager, C. (1992), Mapping vegetation types with the multiple spectral feature mapping algorithm in both emission and absorption, in *Summaries of the Third Annual JPL Airborne Geoscience Workshop, June 1–5, 1992: Volume 1. AVIRIS Workshop* (R. O. Green, Ed.), JPL Publication 92-14, Jet Propulsion Laboratory, Pasadena, CA, pp. 60–62.

Conel, J. E., and Alley, R. E. (1985), Lisbon Valley, Utah, uranium test site report, The Joint NASA / Geosat Test Case Project (H. N. Paley, Ed.).

Conel, J. E., Green, R. O., Vane, G., Bruegge, C. J., and Alley, R. E. (1987), AIS-2 radiometry and a comparison of methods for the recovery of ground reflectance, in *Proc. 3rd Airborne Imaging Spectrometer Data Analysis Workshop* (G. Vane, Ed.), JPL Publication 87-30, Jet Propulsion Laboratory, Pasadena, CA, pp. 18–47.

Crowley, J. K. (1990), Techniques for AVIRIS data normalization in areas with partial vegetation cover, in *Proc. 2nd Airborne Visible / Infrared Imaging Spectrometer (AVIRIS) Workshop* (R. O. Green, Ed.), JPL Publication 90-54, Jet Propulsion Laboratory, Pasadena, CA, pp. 192–198.

Gao, B. C., Kierein-Young, K. S., Goetz, A. F. H., Westwater, E. R., Stankov, B. B., and Birkenheuer, D. (1991), Case studies of water vapor and surface liquid water from AVIRIS data measured over Denver, CO and Death Valley, CA, in *Proc. 3rd Airborne Visible / Infrared Imaging Spectrometer (AVIRIS) Workshop* (R. O. Green, Ed.), JPL Publication 91-28, Jet Propulsion Laboratory, pp. 222–231.

Gillespie, A. R., Smith, M. O., Adams, J. B., Willis, S. C., Fischer, A. F., III, and Sabol, D. E. (1990), Interpretation of residual images: Spectral mixture analysis of AVIRIS images, Owens Valley, California, in *Proc. 2nd Airborne Visible / Infrared Imaging Spectrometer (AVIRIS) Workshop* (R. O. Green, Ed.), JPL Publication 90-54, Jet Propulsion Laboratory, Pasadena, CA, pp. 243–270.

Goetz, A. F. H. (1987), The Portable Instant Display and Analysis Spectrometer (PIDAS), in *Proc. 3rd Airborne Imaging Spectrometer Data Analysis Workshop* (G. Vane, Ed.), JPL Publication 87-30, Jet Propulsion Laboratory, Pasadena, CA, pp. 8–17.

Green, R. O., Vane, G., and Conel, J. E. (1988), Determination of in-flight AVIRIS spectral, radiometric, spatial and signal-to-noise characteristics using atmospheric and surface measurements from the vicinity of the rare earth bearing carbonatite at Mountain Pass, California, in *Proc. Airborne Visible / Infrared Imaging Spectrometer (AVIRIS) Performance Evaluation Workshop* (G. Vane, Ed.), JPL Publication 88-38, Jet Propulsion Laboratory, Pasadena, CA, pp. 162–184.

Green, R. O. (1990), Radiative transfer based retrieval of reflectance from calibrated radiance imagery measured by an imaging spectrometer for lithological mapping of the Clark Mountains, California, *Imaging Spectroscopy of the Terrestrial Environment*, SPIE 1298, pp. 213–221.

Green, R. O. (1991), Retrieval of reflectance from AVIRIS measured radiance using a radiative transfer code, in *Proc. 3rd Airborne Visible / Infrared Imaging Spectrometer (AVIRIS) Workshop* (R. O. Green, Ed.), JPL Publication 91-28, Jet Propulsion Laboratory, Pasadena, CA, pp. 200–210.

Green, R. O., Conel, J. E., Margolis, J. S., Bruegge, C. J., and Hoover, G. (1991), An inversion algorithm for retrieval of atmospheric and leaf water absorption from AVIRIS radiance with compensation for atmospheric scattering, in *Proc. 3rd Airborne Visible / Infrared Imaging Spectrometer (AVIRIS) Workshop* (R. O. Green, Ed.), JPL Publication 91-28, Jet Propulsion Laboratory, Pasadena, CA, pp. 51–61.

Green, R. O., Conel, J. E. Bruegge, C. J., Margolis, J. S., Carrere, V., Vane, G., and Hoover, G. (1992), In-flight

calibration of the spectral and radiometric characteristics of AVIRIS in 1991, in *Summaries of the Third Annual JPL Airborne Geoscience Workshop, June 1–5, 1992: Volume 1. AVIRIS Workshop* (R. O. Green, Ed.), JPL Publication 92-14, Jet Propulsion Laboratory, Pasadena, CA, pp. 1–4.

Green, R. O., Conel, J. E., and Chrien, T. G. (1993), Correction of AVIRIS radiance to reflectance using MODTRAN 2, *Imaging Spectrometry of the Terrestrial Environment*, SPIE 1937, forthcoming.

Kneizys, F. X., Shettle, E. P., Anderson, G. P., Abrew, L. W., Chetwynd, J. H., Shelby, J. E. A., and Gallery, W. O. (1989), *Atmospheric Transmittance / Radiance; Computer Code LOWTRAN 7*, AFGL Hanscom AFB, Bedford, MA.

Mustard, J. F., and Pieters, C. M. (1989), Photometric phase functions of common geologic minerals and applications to quantitative analysis of mineral mixture reflectance spectra, *J. Geophys. Res.* 94:13,619–13,634.

Roberts, D. A., Yamagushi, Y., and Lyon, R. J. P. (1986), Comparison of various techniques for calibration of AIS data, in *Proc. 2nd Airborne Imaging Spectrometer Data Analysis Workshop* (G. Vane and A. F. H. Goetz, Eds.), JPL Publication 86-35, Jet Propulsion Laboratory, Pasadena, CA, pp. 21–30.

Singer, R. B., and McCord, T. B. (1979), Mars: Large scale mixing of bright and dark surface materials and implications for analysis of spectral reflectance, in *Proc. Lunar Planet. Sci. Conf. 10th*, pp. 1835–1848.

Smith, M. O., Roberts, D. A., Shipman, H. M., Adams, J. B., Willis, S. C., and Gillespie, A. R. (1987), Calibrating AIS images using the surface as a reference, in *Proc. Third Airborne Imaging Spectrometer Data Analysis Workshop* (G. Vane, Ed.), JPL Publication 87-30, Jet Propulsion Laboratory, Pasadena, CA, pp. 63–69.

Smith, M. O., Ustin, S. L., Adams, J. B., and Gillespie, A. R. (1990), Vegetation in deserts: 1. A regional measure of abundance from multispectral images. *Remote Sens. Environ.* 31:1–26.

Vane, G. (1987), First results from the Airborne Visible / Infrared Imaging Spectrometer (AVIRIS), *Proc. SPIE* 834: 166–174.

Vane, G., and Goetz, A. F. H. (1988), Terrestrial imaging spectroscopy, *Remote Sens. Environ.* 24:1–29.